A. Haarahiltunen, H. Väinölä, O. Anttila, M. Yli-Koski, and J. Sinkkonen, Modeling and optimization of internal gettering of iron in silicon, ECS Transactions Vol. 3 (4), Editors: C. L. Claeys, M. Watanabe, R. Falster and P. Stallhofer, p 273-284 (2006).

© 2006 The Electrochemical Society (ECS)

Reproduced by permission of The Electrochemical Society (ECS).

**Modeling and optimization of internal gettering of iron in silicon**

A. Haarahiltunen, H. Väinölä, M. Yli-Koski, and
J. Sinkkonen
Helsinki University of Technology, P.O. BOX 3500, FI- 02015 TKK, Finland

O. Anttila
Okmetic Oyj, P.O. BOX 44, 01301 Vantaa, Finland

## Abstract

We present a model for heterogeneous precipitation of iron in silicon. In the model Fokker-Planck Equation is used to simulate the evolution of size distribution of iron precipitates. From the simulation results we may conclude, that in case of low levels of initial iron concentration ($<1\times10^{12}$ cm$^{-3}$), internal gettering is difficult to achieve just by cooling. The low level of initial iron concentration can be gettered by using an additional nucleation step, which can be just a fast ramp to room temperature, before isothermal gettering anneal. We also analyze the effect of competitive gettering on the final iron concentration and the iron precipitate density profile. We found that internal gettering can reduce iron concentration and the particular advantage is the reduction of the iron precipitate density in the device layer. The iron precipitation in the device layer can also be reduced by increasing the doping concentration as the segregation increases.

## Introduction

In silicon one of the most troubling and common contaminant is iron. It is relatively fast diffusing and has deleterious effects on device performance even when present in small concentrations. As experimental process optimization for the impurity gettering is expensive and time consuming, several theoretical papers (1,2,3,4,5,6,7) discuss modeling of gettering of iron. In these papers the iron precipitation to oxide precipitates is usually modeled by Ham's law (8) and it is further assumed that all oxide precipitates are effective (active) gettering sites, i.e. all of the oxide precipitates contain iron precipitate(s). It is experimentally confirmed that using Ham's law the iron precipitation can be described at very high supersaturation (1,9). The simulations greatly overestimate the gettering efficiency of slowly cooled samples (10), when Ham's law and oxide precipitate density is used. A better agreement between simulation and experimental results was achieved by using a significantly lower effective gettering site density than oxide precipitates density (10). This means that nucleation of iron precipitates must be taken into account and the number of effective gettering sites might be only small portion (1,11,12) of the total oxide precipitate density.

In Refs. 6 and 7 the nucleation is taken into account by a using steaty-state nucleation rate and it is shown that the iron precipitation can be simulated at low supersaturation. However, handling a size distribution of iron precipitates is difficult in the steady state approach. The proper handling of size distribution of iron precipitates is especially important when a more complex process than cooling or isothermal anneal is simulated. We had recently suggested the model for heterogeneous precipitation of iron in silicon (13) in which we use the Chemical Rate Equations (CRE) to calculate the size

distribution of iron precipitates and residual iron concentration. In the present work we discuss the modeling and optimization of the internal gettering process.

## Modeling of Heterogeneous Precipitation of Iron

The CRE can be solved using the selected grid point method (14) as we have done before in Ref. (13). This solution is rather time consuming, thus we use the Fokker-Planck Equation (FPE) to simulate the evolution of the size distribution of iron precipitates

$$\frac{\partial f(n,t)}{\partial t} = \frac{\partial}{\partial n}\left( - A(n,t) f(n,t) + B(n,t) \frac{\partial f(n,t)}{\partial n} \right), \qquad [1]$$

where $f(n,t)$ is the density of heterogeneous precipitation sites containing $n$ atoms of precipitated iron and

$$A(n,t) = g(n,t) - d(n,t) \text{ and } B(n,t) = \frac{g(n,t) + d(n,t)}{2} \qquad [2]$$

where $g(n,t)$ and $d(n,t)$ are growth and dissolution rates, respectively. The growth and dissolution rates are (13)

$$g_n = 4\pi r_{ox} D C_{\mathrm{Fe}} \text{ and } d_n = 4\pi r_{ox} D C_{eq} . \qquad [3]$$

where $r_{ox}$ is the average radius of the oxide precipitates, $D$ is the diffusion constant of iron, $C_{\mathrm{Fe}}$ is the interstitial iron concentration and $C_{eq}$ is the equilibrium iron concentration at the interface of the gettering site. We presume that the equilibrium iron concentration at the interface depends on the number of iron atoms precipitated to the gettering site and has the form (13)

$$C_{eq} = C_{eff} \exp\left( \frac{E_a}{kTn^{1/2}} \right), \qquad [4]$$

where $E_a/n^{1/2}$ describes the fact that iron has a higher chemical potential in a small cluster than in a large cluster and $C_{eff}$ is the equilibrium concentration at the interface of a very large iron precipitate. $E_a$ is fitting parameter which is related to surface energy and includes also possible effect of the strain (15,16,17) and the morphology () of oxide precipitates as well as the charge state (18) of iron.

The practical numerical solution of FPE is given in Ref. 19. The solution of FPE requires boundary condition at size one, which is set to

$$f_1 = P_1 f_0 \exp\left( \frac{kT \log\left( \frac{C_{Fe}}{C_{eff}} \right) - 2E_a}{kT} \right), \qquad [5]$$

which is actually the size distribution function for a quasi-equilibrium state in a ideal heterogeneous nucleation process adjusted with fitting parameter $P_1$.

In the fitting we used $Ceff$=4.3×10$^{22}$exp(-2.10eV/$kT$) cm$^{-3}$ (20) and the fitted parameters are $P_1$=1×10$^4$, $E_a$=(1.015×10$^{-4}$$T$+0.8033) eV, $T$<500 ºC and $E_a$=(6.038$T$×10$^{-4}$$T$ +0.4150 )eV, T≥500 ºC (21). In the simulations, in which the denuded zone DZ (or oxide precipitate free zone) or the boron doped layer is included, diffusion and segregation are calculated by a algorithm which described in detail in Ref. 2. The solubility of iron as function of boron doping is calculated as in Ref. 22. The effect of trapping of interstitial ionized iron by boron on the diffusivity of iron is calculated as suggested in Ref. 23.

## Results and Discussion

### Effective Gettering Site Density

Nakamura et. al. (6) used the experimental results of Hieslmaier (1) et. al. to fit their model parameters as isothermal anneal. However, in experiments significant nucleation of iron precipitates can occur during quenching to room temperature after contamination. Therefore parameters should be fitted using experimental results where the room temperature (RT) step is avoided as we have done in Ref. (21). In Fig. 1 is shown the effect of quenching, which is taken as cooling 25 K/s to room temperature, on iron precipitate density (≈ effective gettering site density). It can be seen that with quenching the simulation and experimental results agree well. Without quenching simulation results drop far below experimental. This is in line with the experimental results of Refs. (10,24,25). This means that nucleation at high temperature is much slower, than is apparent from results showed in Fig. 1, as the measured effective gettering site density is strongly affected by nucleation during fast ramps.

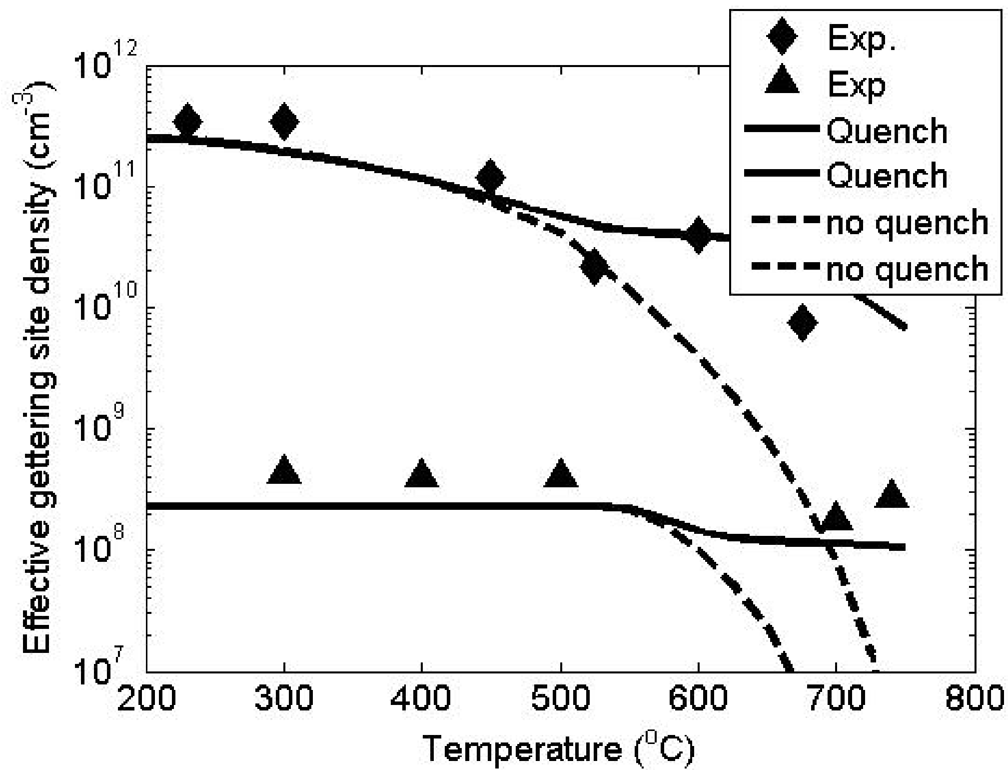


Fig. 1. Relationship between the temperature and the density of effective gettering sites with various oxygen precipitate states, triangle $2.3\times10^{8}$ $cm^{-3}$ 83.8 nm and diamond $2.5\times10^{11}$ $cm^{-3}$ 22.5 nm are experimental results from Ref. (1). The dashed lines corresponds to simulations without quenching and the solid lines with quenching.

Gettering by Cooling

Fig. 2 shows the experimental (10,24) and simulation results of slow cooling (2 $^{o}C/min$) from 850 $^{o}C$ to different pull out temperatures with initial iron concentrations of $1.3\times10^{13}$ and $2.2\times10^{13}$ $cm^{-3}$. In these simulations DZ is 50 µm, the radius of oxide precipitate is 76 nm and oxide precipitate density in bulk is $2\times10^{10}$ $cm^{-3}$. In the DZ the oxide precipitate density and radius are set to $5\times10^{8}$ $cm^{-3}$ and 0.2 nm, respectively, as estimated by Hieslmaier et. al.. The oxide precipitates density and size in bulk and in DZ is kept constants throughout the whole paper. It is interesting to analyze gettering efficiency as a function of cooling rate and initial iron concentration level as the results of Fig. 2 indicate that the gettering efficiency is strongly depended on initial iron concentration. In these simulations DZ is set to 20 µm. The simulation results are presented in Fig. 3. We may conclude that the only high initial iron concentrations, above $1\times10^{13}$ $cm^{-3}$, can be gettered simply by pulling out of furnace i.e. high cooling rate. The gettering of low level iron concentration, below $1\times10^{12}$ $cm^{-3}$, is impossible at any realistic cooling rates. This is because sufficiently high supersaturation level and diffusivity are not reached simultaneously under these processing conditions.

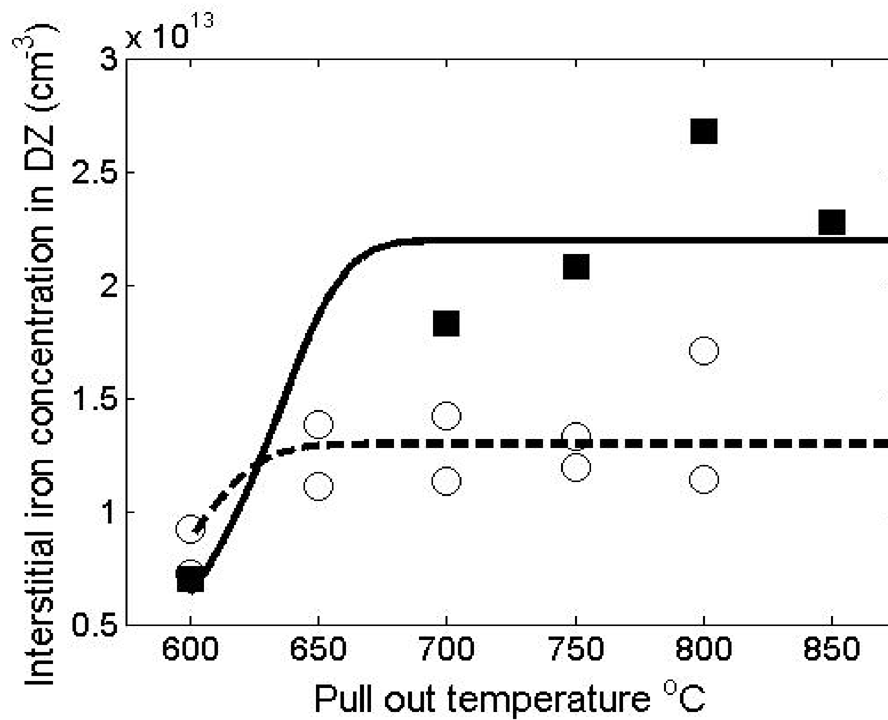


Fig. 2. Experimental results of slow cooling (2 °C/min) from 850 °C to pull out temperature are taken from reference (10) (squares) and (24) (open circles). . In the simulated results the initial iron concentration is $2.2\times10^{13}$ cm$^{-3}$ (solid line) or $1.3\times10^{13}$ cm$^{-3}$ (dashed line).

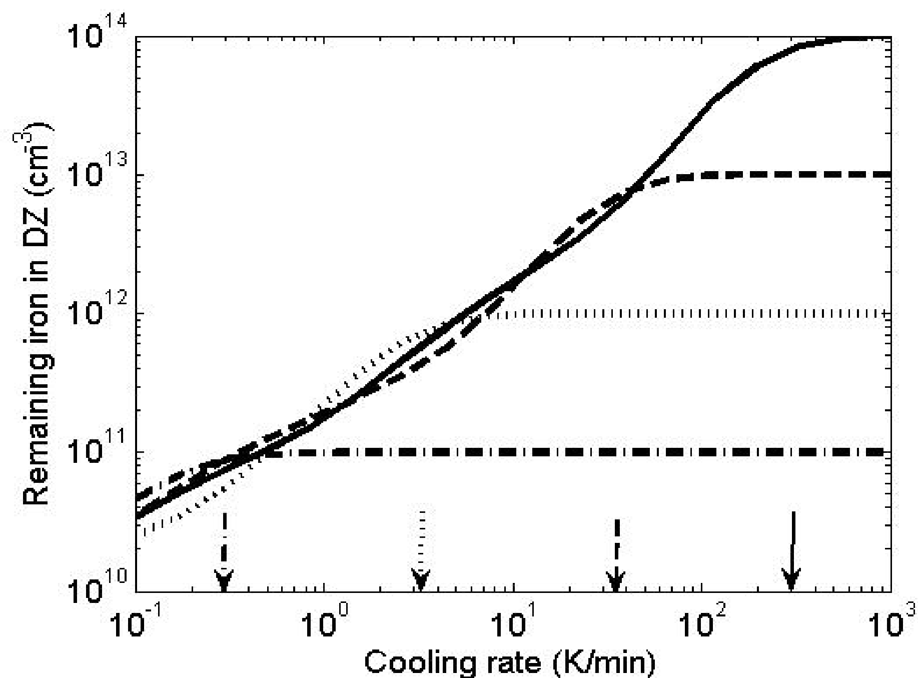


FIG. 3. The remaining iron in the DZ versus the linear cooling rate. The cooling is done from 1000 to 200 ºC. The initial iron concentrations were $1\times10^{14}$ (solid line), $1\times10^{13}$ (dashed line), $1\times10^{12}$ (dotted line) and $1\times10^{11}$ cm$^{-3}$ (dashed-dotted line). Arrows mark the cooling rates where gettering starts at each initial iron concentration.

Nucleation anneal

The problems in gettering of low level iron concentration by cooling might be overcome by using a low temperature nucleation anneal as we have demonstrated (25) for contamination level 1-2×$10^{13}$ $cm^{-3}$. In our experiments the wafers were divided into two different gettering treatments: i) In the first treatment the wafers were annealed at 900 °C and then slowly cooled to 700 °C where the isothermal gettering anneal was performed. ii) In the second treatment the wafers were pulled out directly from 900 °C, air cooled to RT, loaded again to 700 °C and annealed further for different times. As shown in Fig. 4 the ramp to RT has a drastic effect on the iron precipitation behavior at 700 °C.

The simulation agrees with the experiments such that no gettering occurs when wafers are annealed at 700 °C after cooling from 900 °C. In the RT step simulation we simulate the RT step as quenching. The simulation predicts a too fast iron precipitation when RT step is included, however, in the experiments the cooling was not quenching. The simulation timescale is closer to the results of Aoki et. al. (20), as they did isothermal gettering using quenched samples.

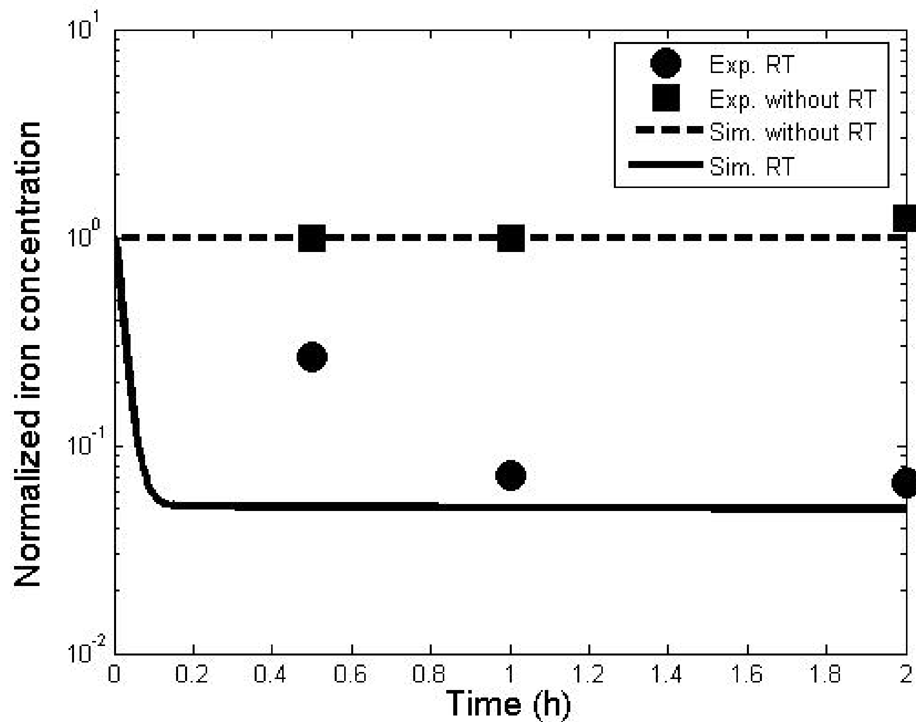


FIG. 4. The interstitial iron concentration dependence on annealing time for 700 °C annealing. The squares are our experimental results (25) without a room temperature step and the circles are experimental results when the RT step is included in the process. The simulated results without the RT step (dashed line) and with the RT step (solid line).

. We studied the effect of nucleation, which was done by ramping 100 K/min to RT and ramp-up to final annealing temperature, on the gettering efficiency of iron at an initial iron concentration of 1×$10^{12}$ $cm^{-3}$. In Fig. 5 the iron gettering efficiency versus annealing time at 550 ºC is compared in two different cases. It can be seen that gettering

is much faster in the case when ramp to RT is included in process and after about 80 minutes the iron concentration reached the solubility. It is obvious that optimal internal gettering cannot be done just by cooling. In real life process the nucleation of iron precipitates most probably occurs during ramps, even the final gettering occurs in some mid-temperature process step.

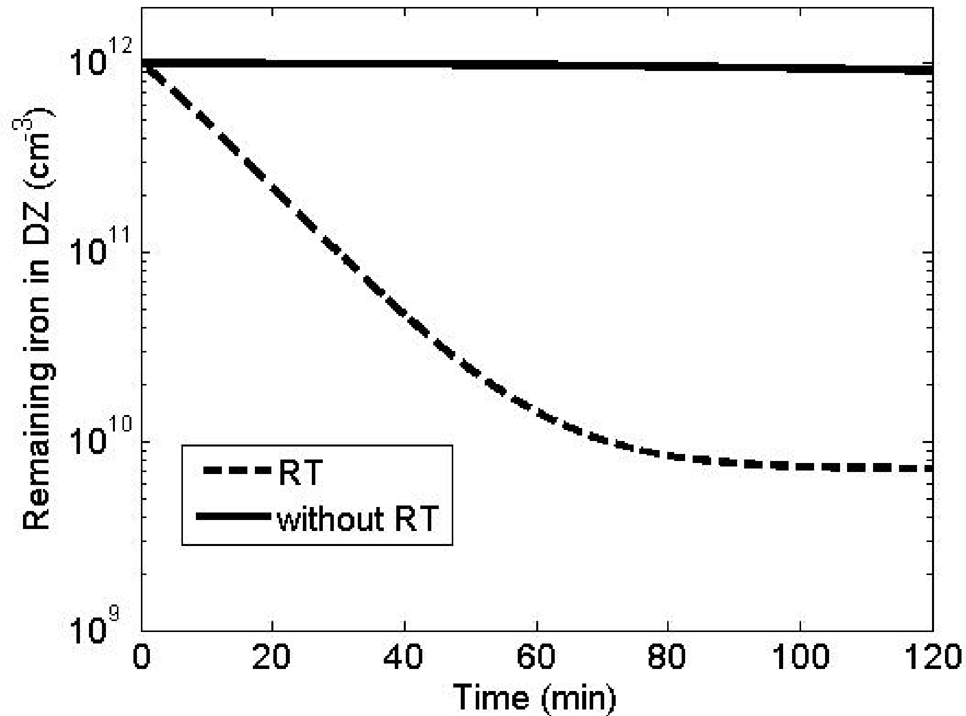


Fig. 5. The comparison of iron gettering by i) cooling 100 K/min to 550 ºC (solid line) and annealing and ii) cooling 100 K/min to RT, loading 100 K/min to 550 ºC and annealing (dashed line). The initial iron concentration was $1\times10^{12}$ $cm^{-3}$.

Competitive gettering

In the previous section we showed how a low temperature nucleation anneal enhance internal gettering. In the example simulations the final gettering was done at 550 ºC where also the segregation to device layer and the precipitation there, i.e. competitive gettering (22), might occur. We repeated the analysis of gettering of a initial iron concentration of $1\times10^{12}$ $cm^{-3}$, when a boron doped three microns thick device layer is included. The concentration of boron doping was $1\times10^{18}$, $1\times10^{19}$ or $1\times10^{20}$ $cm^{-3}$. The doping profiles and defect density profiles are shown in Fig. 6. In the device layer we use an effective radius of 10 nm and a density of $1\times10^{9}$ $cm^{-3}$ to take into account the iron precipitation due to residual damage from ion implantation. The effect of boron doping on iron precipitation was taken into account by changes

$$C_{eff}(B) = k_{Seg}(B)C_{eff} \quad \text{and} \quad D = D(B) \qquad [6]$$

where $k_{Seg}$ is the segregation coefficient (22), D(B) is the effective diffusion constant of iron (23) and $B$ is the boron concentration. The other parameters were kept constant although it is possible that the fitting parameters have a doping concentration

dependency. The boron doping increases the solubility and decreases the diffusivity, thus at a given initial iron concentration the iron precipitation is retarded as the boron concentration is increased.

Istratov et. al. pointed out that metals become detrimental when they agglomerate in relatively weakly doped areas, or form precipitates in the device layer which also penetrate iton weakly doped regions or at the gate oxide interface. Thus, in the simulation we are interested in the total iron concentration and the density of iron precipitates as a function of depth after a two hour gettering.

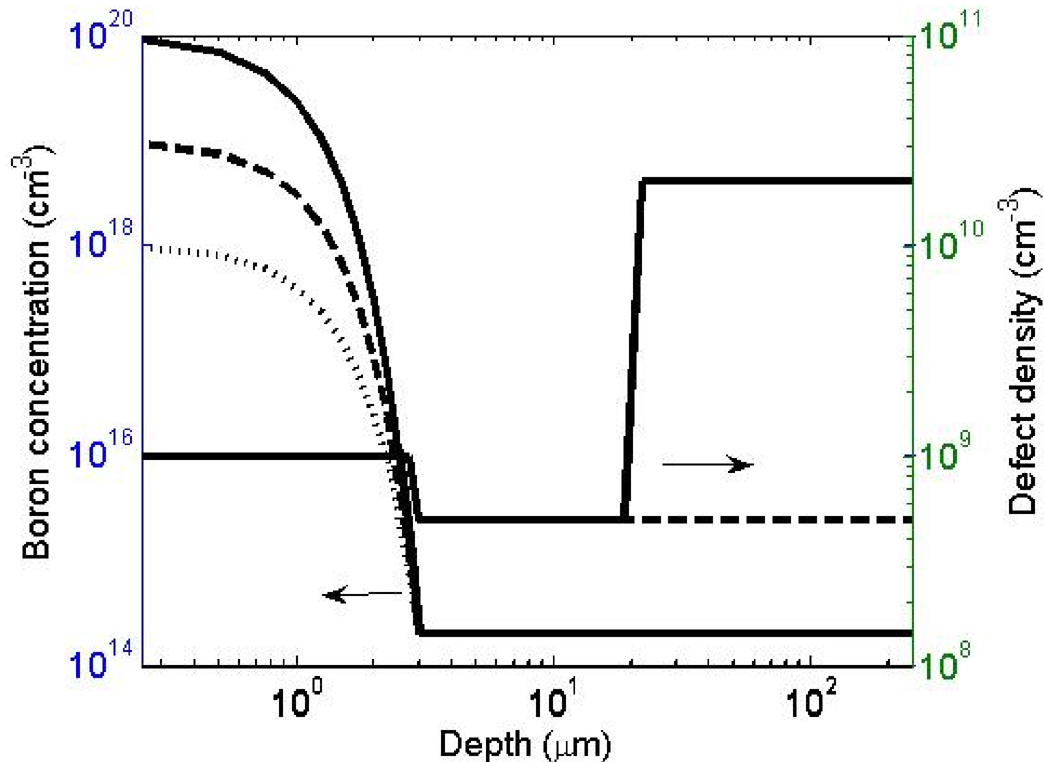


FIG. 6. The doping and defect density profiles used in competitive gettering simulations

The simulation results are shown in Fig.7. The residual iron concentration in the device layer is in all cases reduced by IG. An important effect is also that the density of iron precipitate in the device layer is reduced by IG. The iron precipitate density in device layer follows the doping concentration profile as the supersaturation is nearly constant the due to high diffusivity in the device layer. This means that boundary condition (Eq. 5) is the same in all point of device layer and growth (dissolution) rates (Eq. 3) are multiplied by the segregation coefficient leading to higher nucleation rates at higher doping concentration. Yet, the total number of iron precipitates decreases when the total boron doping increases, as the segregation coefficient increases and the supersaturation in the device layer decreases.

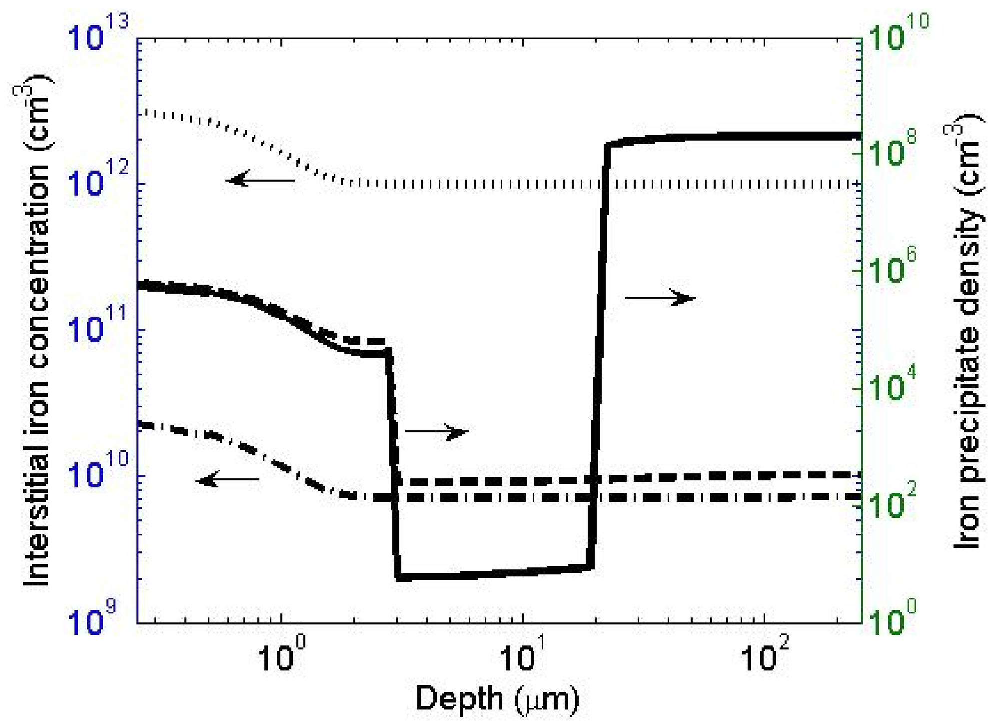


a)

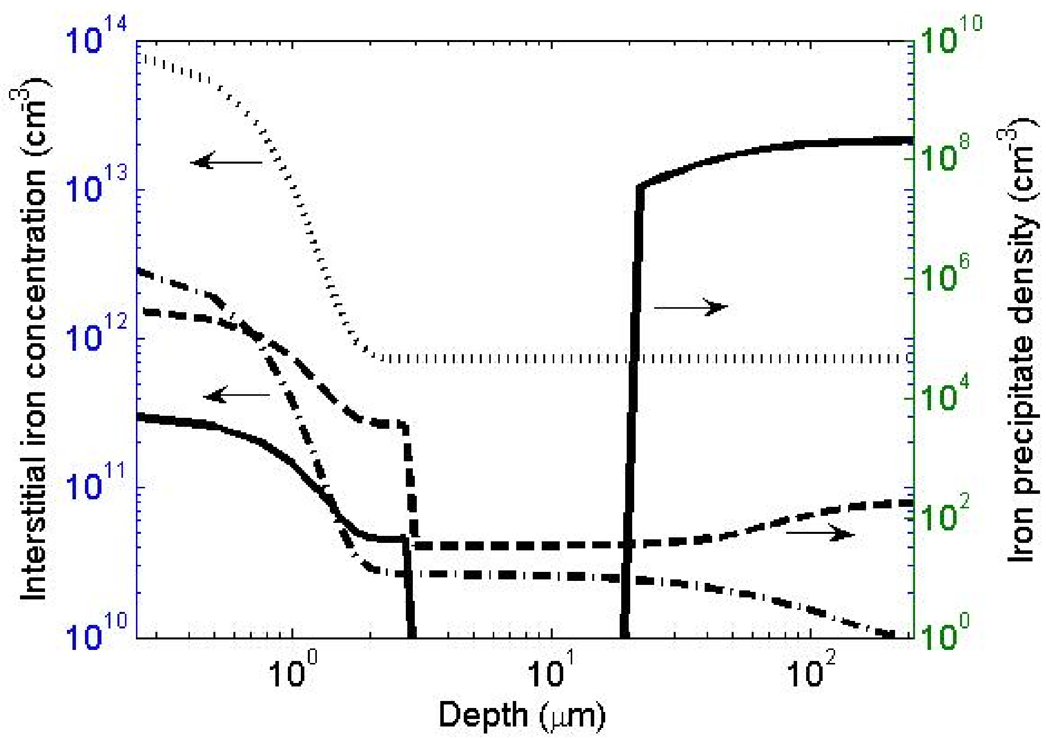


b)

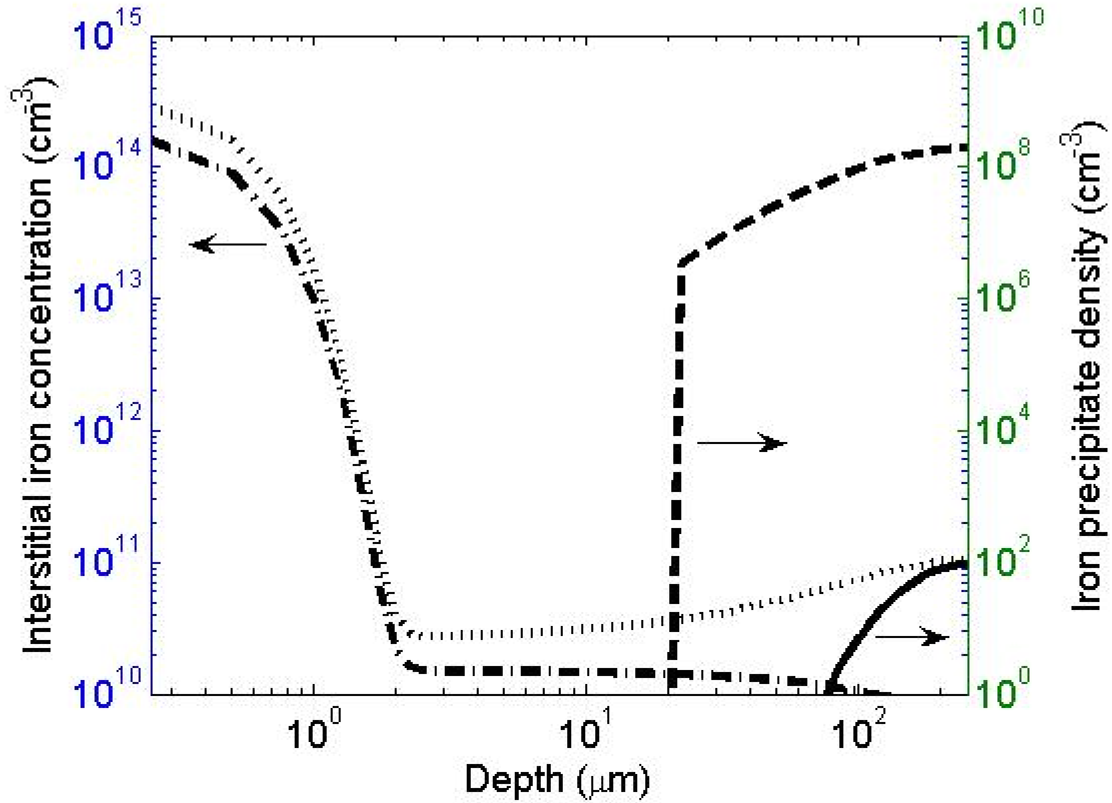


c)

FIG. 7. Results of iron gettering by cooling 100 K/min to RT, loading 100 K/min to 550 ºC when the device layer is included. The boron concentration was a) $1\times10^{18}$ cm$^{-3}$ , b) $1\times10^{19}$ cm$^{-3}$ and c) $1\times10^{20}$ cm$^{-3}$. The iron concentration without IG (dotted line), the iron concentration with IG (dash-dotted line), iron precipitate density without IG (solid line) and iron precipitate density with IG (dashed line) The initial iron concentration was $1\times10^{12}$ cm$^{-3}$.

The simulations were repeated using initial iron concentrations $1\times10^{13}$ and $1\times10^{14}$ cm$^{-3}$. The results can be summarised as follows. The difference between non-IG and IG samples grows when iron concentration increases. However, at the same time the total iron precipitate density in the device layer also increases. The effect of IG was observed also after ramp down at an iron concentration of $1\times10^{14}$ cm$^{-3}$ (see Fig. 3). None of the boron concentrations completely suppress iron precipitation in device layer at iron concentrations of $1\times10^{13}$ or $1\times10^{14}$ cm$^{-3}$.

**Conclusion**

The internal gettering of iron at low levels of initial iron concentration (<$1\times10^{12}$ cm$^{-3}$) is difficult just by (slow) cooling. The low temperature nucleation anneal is needed to induce a significant number of iron precipitates which further grow and getter iron at higher temperature. The nucleation step can be a fast ramp, even quenching, and this effect was not usually been taken into account in past experiments and analysis of iron precipitation. For optimal IG the proper combination of nucleation and growth steps of iron precipitates must be found. In practice the growth step can be in a temperature range,

in which a competitive gettering by a heavily doped device layer is significant. In this case the particular advantage of IG is the reduction of the iron precipitate density in the device layer. Also the segregation to the device layer reduced, and may even completely prevent the iron precipitation in device layer at low levels of initial iron concentration.

## Acknowledgements

The authors acknowledge the financial support from the Finnish National Technology Agency, Academy of Finland, Okmetic Oyj, Micro Analog Systems Oy and VTI Technologies Oy.

## References

1. H. Hieslmair, A. A. Istratov, S. A. McHugo, C. Flink, T. Heiser, and E. R. Weber, *Appl. Phys. Lett.* **72**, 1460 (1998).
2. H. Hieslmair, S. Balasubramanian, A. A. Istratov, and E. R. Weber, *Semicond. Sci. Technol.* ***16***, 567 (2001).
3. A. L. Smith, K. Wada, and L. C. Kimerling, *J. Electrochem. Soc*. **147**, 1154 (2000).
4. T. Y. Tan, R. Gafiteanu, S. M. Joshi, and U. Gösele, in *Semiconductor silicon 1998*, edited by H. Huff, U. Gösele, and H. Tsuya (The Electrochemical Society, Pennington, NJ, 1998), p. 1050.
5. H. Hieslmaier, A. A. Istratov and E. R. Weber, *Semicond. Sci. Technol.* **13**, 1401 (1998).
6. K. Nakamura and J. Tomioka, *ECS Transactions* **2** (2), 275-286 (2006)
7. P. Geranzani, M. Pagani, C. Pello, and G. Borionetti, *Solid State Phen.* **82-84**, 381 (2002).
8. F. S. Ham, *J. Phys. Chem. Solids* **6**, 335 (1958).
9. D. Gilles, E. R. Weber, and S. Hahn, *Phys. Rev. Lett*. **64**, 196 (1990).
10. A. Haarahiltunen, M. Yli-Koski, H. Väinölä, M. Palokangas, E. Saarnilehto, and J. Sinkkonen, *Physica Scripta* **T114**, 88 (2004).
11. R. J. Falster, G. R. Fisher, and G. Ferrero, Appl. Phys. Lett. **59**, 809 (1991).
12. R. Falster, in *Crystalline Defects and Contamination: Their impact and Control in Device Manufacturing,* Proceeding of the Satellite Symposium to ESSDERC 93 Grenoble, France, edited by B. O. Kolbesen, C. Claeys, P. Stallhofer, and F. Tardif (The Electrochemical Society, Pennington, NJ, 1993), pp. 149-169.
13. A. Haarahiltunen, H. Väinölä, O. Anttila, E. Saarnilehto, M. Yli-Koski, J. Storgårds, and J. Sinkkonen, *Appl. Phys. Lett*. **87**, 151908 (2005).
14. S. Kobayashi, *J. Crystal Growth* **174**, 163 (1997).
15. H. Takahashi, H. Yamada-Kaneta, and M. Suezawa, *Jpn. J. Appl. Phys.* **37**, 1689 (1998).
16. J. Vanhellemont and C. Claeys, *Mater. Sci. Forum* **38**, 171 (1989).
17. S. A. McHugo, E. R. Weber, M. Mizuno and F. G. Kirscht, *Appl. Phys. Lett.* **66**, 2840 (1995).
18. A. Mesli, T. Heiser, N. Amroun, and P. Siffert, *Appl. Phys. Lett.* **57** 1898 (1990).
19. J. S. Chang, and G. Cooper, *J. Comp. Phys.* **6**, 1 (1970).
20. M. Aoki and A. Hara, J. Appl. Phys. **74**, 1440 (1993).
21. A. Haarahiltunen, H. Väinölä, O. Anttila, M. Yli-Koski, and J. Sinkkonen, to be published in J. Appl. Phys..

22. A. A. Istratov, W. Huber, and E. R. Weber, *J. Electrochem. Soc.* **150**, G244 (2003).
23. H. Kohno, H. Hieslmaier, A. A. Istratov, and E. R. Weber, *Appl. Phys. Lett.* **76**, 2734 (2000).
24 A. Haarahiltunen, H. Väinölä, M. Yli-Koski, E. Saarnilehto and J. Sinkkonen, in *High purity silicon VIII,* Proceedings of The Electrochemical Society Fall 2004 Meeting Honolulu, USA, edited by C. L. Claeys, M. Watanabe, R. Falster and P. Stallhofer, (The Electrochemical Society, Pennington, NJ, 2004), pp. 135-145.
25 H. Väinölä, A. Haarahiltunen, M. Yli-Koski, E. Saarnilehto, and J. Sinkkonen, in *High purity silicon VIII,* Proceedings of The Electrochemical Society Fall 2004 Meeting Honolulu, USA, edited by C. L. Claeys, M. Watanabe, R. Falster and P. Stallhofer, (The Electrochemical Society, Pennington, NJ, 2004), pp. 160-164.